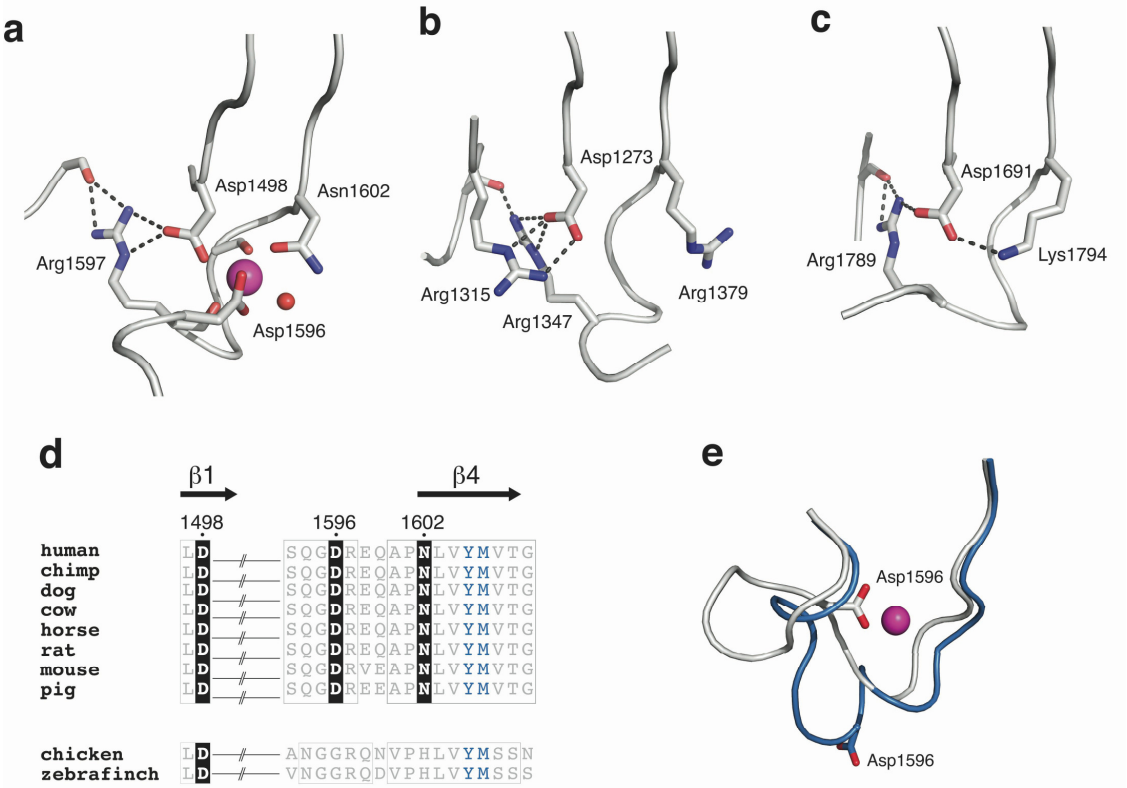

Supplementary Figure S1 The calcium-binding site of VWF-A2. Close up of the $\alpha_3\beta_4$ loop of (**a**) VWF-A2, (**b**) VWF-A1 and (**c**) VWF-A3. In all VWF-A domains, $\alpha_3\beta_4$ is anchored via electrostatic interaction between a conserved aspartate in β_1 and a conserved arginine in the $\alpha_3\beta_4$ loop. In agreement with our results from thermal stability assays structural comparison shows that among the VWA domain repeat, metal binding functionality at this site is unique to A2. In A2 calcium binds to a negatively charged pocket formed by the $\alpha_3\beta_4$ loop. In A1 and A3, the positively charged side chains of A1-Arg1374 and A3-Lys1794, which replace A2-Asn1602, point into the cavity formed by the $\alpha_3\beta_4$ loop, obliterating calcium binding by charge repulsion. Key side chains are shown as sticks; calcium ion, magenta sphere; H_2O, red sphere. (**d**) Asp1596 and Asn1602 that coordinate calcium through side chain atoms are strictly conserved in mammalian, but absent from avian VWF sequences. (**e**) Calcium coordination by A2 leads to a marked rearrangement of the $\alpha_3\beta_4$ loop triggered by Asp1596, which moves more than 16 Å to coordinate the calcium ion. Asp1596 and Asn1602 that coordinate calcium through side chain atoms are strictly

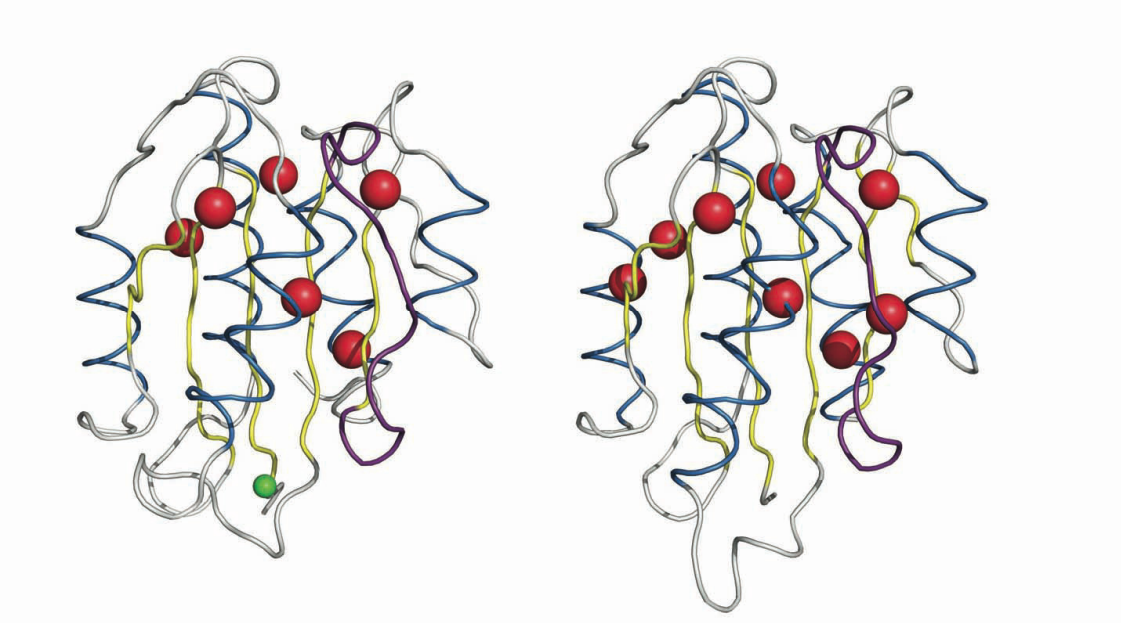

Supplementary Figure S2 Global packing analysis of calcium-bound A2 (left) and calcium-free A2 (right; PDB 3GXB). A Voronoi cell algorithm[59] was applied to determine local packing densities and interior cavities. The α_4-less loop is shown in purple; the calcium ion in green; local cavities due to packing defects are depicted as red spheres. Both structures show similar packing defects on either side of the central beta sheet, indicating that the stabilizing effect observed by calcium binding is not due to overall improvement of side chain packing.

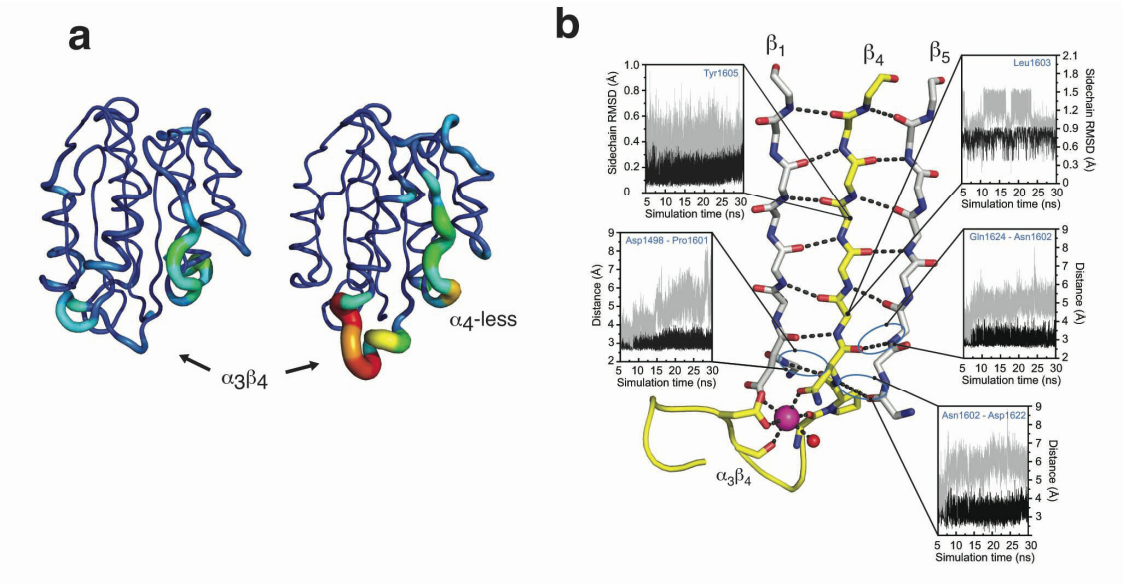

Supplementary Figure S3 Calcium binding modulates dynamics of $\alpha_3\beta_4$ and scissile strand β_4. (**a**) Root mean square fluctuations of the protein main chain averaged over three independent 30 ns molecular dynamics simulations are projected onto the tube representation of the backbone traces of calcium-bound (left) and calcium-free (right) A2. Rmsf amplitudes are represented by tube diameter and color-coded by decreasing amplitude from red (4 Å) to blue (0.3 Å). Consistent with the experimental B-factor distributions in the calcium-free system we observe highest rmsf values for the $\alpha_3\beta_4$ and α_4-less loops that both flank the scissile strand. In particular, the $\alpha_3\beta_4$-loop deviates markedly from the reference conformation of the starting structure. As anticipated, this loop is significantly less flexible in the calcium-bound ensemble. It can be appreciated that the large movements of the flanking loop regions in the calcium-free structure impose substantial strain on the β_4-strand. This is reflected by the quality of hydrogen bonds formed during the simulation between β_4 and its neighboring strands. (**b**) Backbone representation of the β_4 scissile strand (yellow) and neighboring strands illustrating how calcium interlocks β_4 with β_1 via coordination by Asp1498 and Asn1602. Also depicted are representative trajectories for selected hydrogen bond donor-acceptor distances and side chain rmsds from molecular dynamics simulations of calcium-free (gray) and calcium-bound (black) A2, showing that metal coordination directly affects the dynamics of scissile strand β_4. Throughout the simulations marked deviations from ideal hydrogen-bond geometries are observed for the calcium-free structures on either side of the β_4 strand.

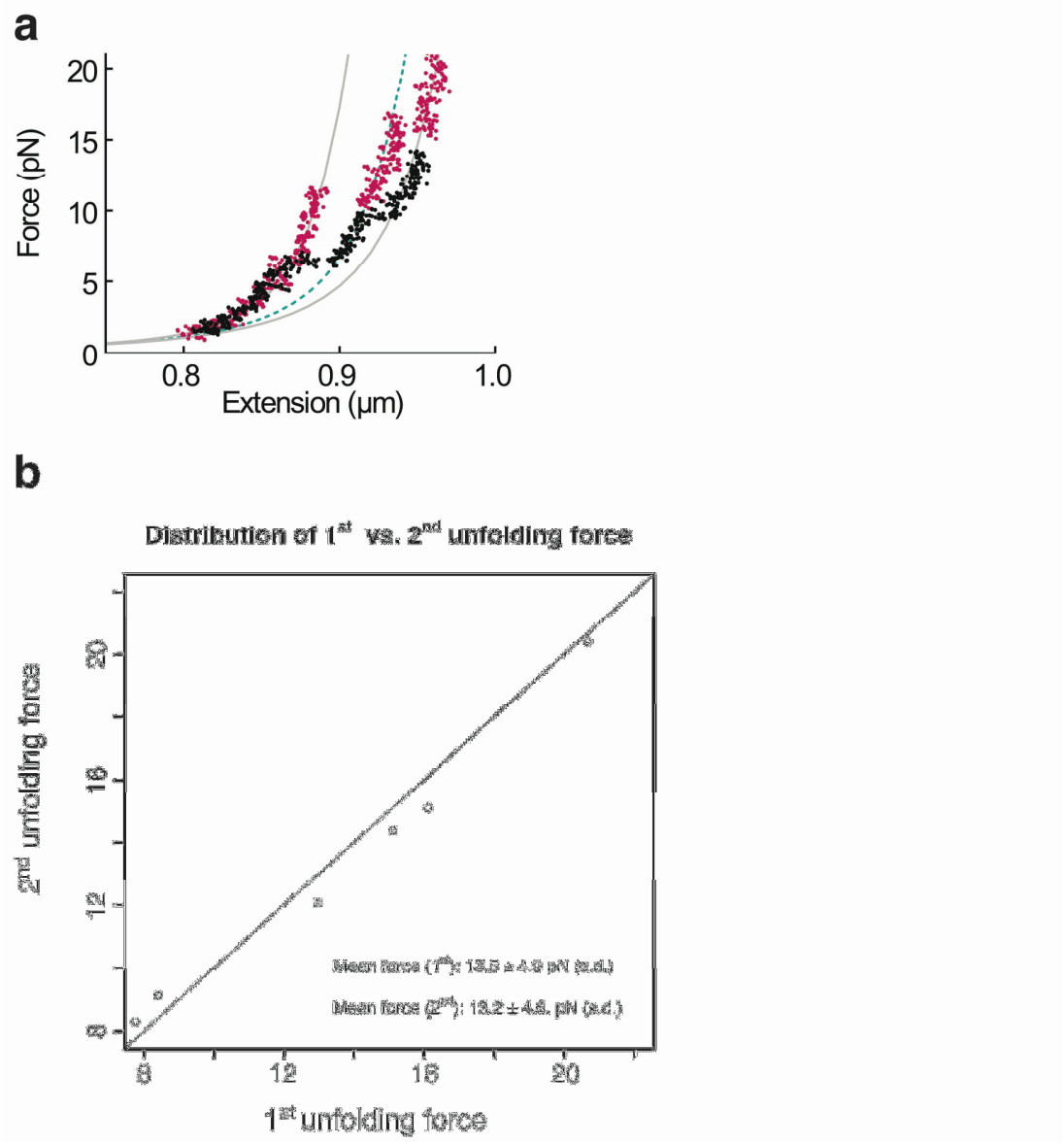

Supplementary Figure S4 Analysis of force spectroscopy data. (**a**) Representative trace for rare unfolding transitions in the presence of EDTA (black) that proceeds via an intermediate. Comparison with a trace in the presence of calcium (red) indicates that the intermediates follow the same WLC. (**b**) Q-Q plot of force distributions obtained from a first stretching experiment and a second stretch after refolding at zero force for A2 with calcium (n1=6, n2=6); mean forces for both distributions are listed. The similarity of force distributions resulting from the first and a second stretch indicate that A2 refolds to the native conformation. In the presence of EDTA mean force for unfolding were 7.8 ± 2.9 pN (s.d.) for the first stretch, and a similar 6.8 ± 3.7 pN (s.d.) after refolding

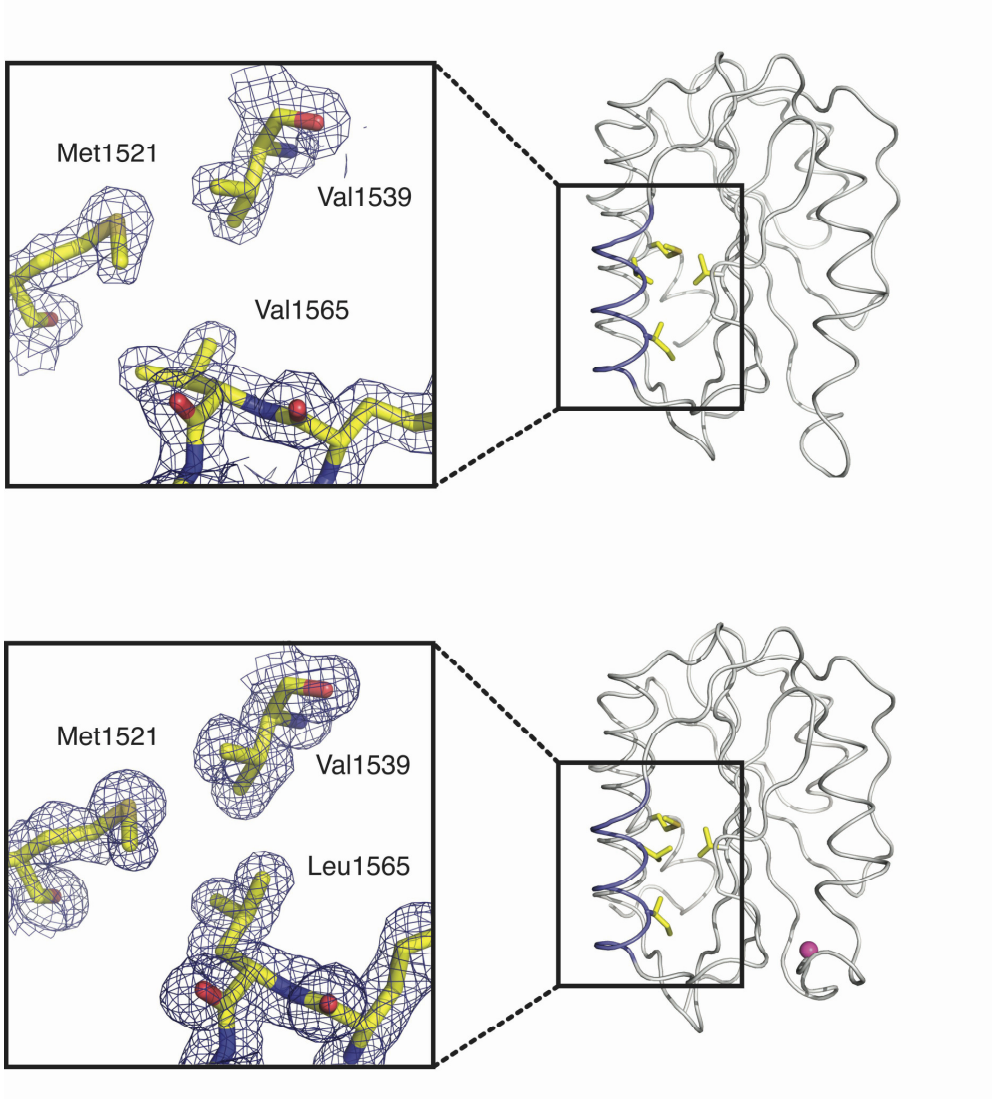

Supplementary Figure S5 Location of the V1565L polymorphism within the A2 structure. We crystallized an A2 variant carrying a 4693G/T single nucleotide polymorphism (SNP), leading to the amino acid substitution V1565L within helix α2. This polymorphism is reported to slightly increase VWF proteolysis[60], but has not been listed as a VWD 2A mutant (www.shef.ac.uk/vwf). Close up of the environment of Val1565 in PDB 3GXB (top) and Leu1565 in calcium-bound A2 (bottom). The right panels show the location of the polymorphism in the overall structure. The α_2-helix is highlighted in purple and important side chains that interact with residue 1565 are shown in yellow. Leu1565 in calcium-bound A2 forms favorable contacts with Met1521 and Val1639, allowing for tighter packing than observed for the wild type Val1565 (left) in PDB 3GXB. This is also evident from the analysis of local packing densities (**Supplementary Fig. S2**), where we find a packing defect for PDB 3GXB at this position. From our analysis we are not able to identify a structural explanation for the observed increase in proteolysis rate of the Leu1565 variant.

Supplementary Table S1: Geometry of the calcium-binding site

Residue	Atom	Monomer A		Monomer B		Monomer C		Reference values (‡)
		Distance (Å)	B (Å^2)	Distance (Å)	B (Å^2)	Distance (Å)	B (Å^2)	Distance (Å)
Asp498	OD2	2.35	9.6	2.37	11.4	2.35	14.1	2.36 ± 0.11
Asp1596	OD1	2.35	12.6	2.35	24.1	2.34	22.7	2.36 ± 0.11
Arg1597	O	2.37	12.8	2.38	10.7	2.38	12.5	2.36 ± 0.13
Ala1600	O	2.35	13.7	2.37	11.0	2.37	13.8	2.36 ± 0.13
Asn1602	OD	2.43	9.1	2.42	9.7	2.42	9.4	2.40 ± 0.11
H_2O	O	2.60	18.7	2.63	25.5	2.62	23.1	2.42 ± 0.16
Calcium	CA		16.2		13.4		16.8	

Supplementary References

59. Rother, K., Hildebrand, P.W., Goede, A., Gruening, B. & Preissner, R. Voronoia: analyzing packing in protein structures. *Nucleic Acids Res.* **37**, 393-395 (2009).

60 Davies J. & Bowen D. An association between the L1565 variant of von Willbrand factor and susceptibility to proteolysis by ADAMTS-13. Haematologica 92, 240-243 (2007)